Available online at www.sciencedirect.com

ScienceDirect

Ocean Engineering 34 (2007) 303–319

OCEAN ENGINEERING

www.elsevier.com/locate/oceaneng

A three-dimensional wave field over a bidirectionally periodic ripple bottom

Chia-Yan Cheng[a], Yang-Yih Chen[b,*], Guan-Yu Chen[c]

[a]*Department of Marine Environment and Engineering, National Sun Yat-sen University, 70 Lien-hai Road, Kaohsiung 804, Taiwan*
[b]*College of Marine Sciences, Department of Marine Environment and Engineering, National Sun Yat-sen University, 70 Lien-hai Road, Kaohsiung 804, Taiwan*
[c]*Institute of Physical Oceanography, National Sun Yat-sen University, 70 Lien-hai Road, Kaohsiung 804, Taiwan*

Received 31 August 2005; accepted 19 December 2005
Available online 19 April 2006

Abstract

For gravity wave trains propagating over an arbitrary wavy bottom, a perturbation expansion is developed to the second order so that the Bragg resonance effect of the ripple bottom on the free-surface wave can be analyzed. Both the resonant and non-resonant cases are treated and the singular behavior at resonance is avoided. This theory is successfully verified by reducing to simpler situations. Then, the analytical results for the special case of a unidirectional sinusoidal bottom are compared with experimental data for validation.

Keywords: Ripple bottom; Perturbation expansion; Bragg resonance

1. Introduction

Periodic topographic variation plays an important role in the evolution of wave motion as they travel from deep sea to shallow water. The first experiment of Heathershaw (1982) showed that a significant amount of wave energy can be reflected from submerged bars if the bar interval is about one-half wavelength of the normally incident waves and that these reflections are due to resonant interactions between surface waves and the bottom topography. Furthermore, the experiment of Davies and Heathershaw (1984) shows that the maximum reflection coefficient increases with the ripple amplitude and decreases with the water depth. Since then, the interaction of surface gravity waves with periodic bottom topography has been investigated extensively through theoretical, experimental and numerical studies. These studies have motivated various ideas for the design of submerged breakwaters that can effectively protect the beach against erosion and have less visual impact on coastal landscapes. From the engineering point of view, it is worthwhile to study the mechanism of this strong reflection of water waves so that a more economical and efficient design of sea-bottom structures in the nearshore zone is possible.

The first theoretical study on the effect of a wave-shaped bottom was given by Jeffreys (1944). He considered a long train of surface waves propagating over a sea bottom of regularly distributed sandbars and studied the variation of the resulting reflection coefficient. Ursell (1947) pointed out that this phenomenon is exactly what is called the Bragg resonance of optics. Davies (1980,1982), Heathershaw (1982) and Davies and Heathershaw (1984) made a series of systematic studies of this topic. They considered incident waves propagating over the ripple bottom with an amplitude small compared with the water depth. By applying linear wave theory, they obtained the reflection coefficient caused by the bottom topography. However, their theoretical results are not applicable at resonance; hence, a proper comparison with their experiments is not available. Mitra and Greenberg (1984) gave the reflection coefficient at resonance, but the coefficient is time-dependent

*Corresponding author.
E-mail addresses: chiayan@mail.nsysu.edu.tw (C.-Y. Cheng), yichen@mail.nsysu.edu.tw (Y.-Y. Chen), guanyu@mail.nsysu.edu.tw (G.-Y. Chen).

0029-8018/$ - see front matter
doi:10.1016/j.oceaneng.2005.12.007

instead of varying from place to place. Thus, a direct comparison with the space-varying reflection coefficient of the experiment is not possible. To overcome this shortcoming, Mei (1985) and Hara and Mei (1987) found a space-varying solution at resonance that is validated by their experiments. Kirby(1986) employed the mild-slope approximation to predict waves propagating over slowly varying topography.

By first introducing two perturbation parameters explicitly, the same problem of regular progressive gravitational water waves propagating over a wavy bottom was solved by Chen and Tang (1990). They assumed the ratio of the wavy bottom amplitude b to the water depth d is small and discussed both the resonant and non-resonant situations. Chen (1991) investigated the growing mechanism in resonance and the same approach is extended to the three-dimensional situation of the present study. An integrated theory containing all kinds of unidirectional wavy bottoms of finite length was developed by Chen (1992) and the theoretical results are validated by comparing with the experimental research of Davies and Heathershaw (1984).

More recently, Charberlain and Porter (1995) developed a decomposition method to obtain the scattering matrix for periodic bottom undulations. Rey et al. (1996) derived an analytical theory for subharmonic Bragg resonance caused by the interaction between small-amplitude surface waves and unidirectional doubly sinusoidal beds. Liu and Yue (1998) studied the generalized Bragg scattering of surface waves over a wavy bottom. On the basis of Phillips' (1960) resonance condition for nonlinear wave–wave interactions, they provided a Bragg resonance condition for second-order and third-order wave–bottom interactions. Cho and Lee (2000) developed a numerical model that contains both propagating and evanescent modes and compared the results with the experiment of Guazzelli et al. (1992). Yu and Mei (2003) gave some numerical calculations and showed that if waves are reflected by both the bottom and the shore, the monotonically decreasing tendency of the spatial wave-energy distribution over the ripple patch will be changed.

The studies mentioned above have concentrated on two-dimensional cases only. Due to the complex sand-dune topography in the coastal zone and the varying direction of incident waves, a three-dimensional study is desirable. By treating normally incident waves whose frequency is slightly different from that of the Bragg resonance, Mei et al. (1988) considered oblique incidence of detuned waves on a finite strip of bars. Zhang et al. (1999) extended the idea of Kirby (1986) and proposed a hybrid model for Bragg scattering of water waves that has both slowly-varying and rapidly varying undulating bottom components. The higher-order terms neglected by Kirby are retained for a better estimate of the reflection coefficient. Porter and Porter (2001) examined the existence of trapped Rayleigh-Bloch waves and the Bragg resonance effect in three-dimensional context by numerical computation in which the mild-slope approximation was employed. However, a complete three-dimensional theory that gives analytic results for wavy periodic bottoms has not been reported yet. In the following, an analytic approach is employed for a thorough understanding of the 3-D Bragg resonance mechanism. By employing three small perturbation parameters, this problem is explicitly solved to the second order exactly without utilizing the mild slope approximation. The accuracy and generality of the solutions are also verified.

2. Formulation of wave motion system

Consider a three-dimensional wave field with undulated bottom form $z = -d + b_1 \cos(\vec{m}_1 \cdot \vec{X} + \varphi) + b_2 \cos(\vec{m}_2 \cdot \vec{X})$ that is constructed by two sinusoidal wave trains of wave number vectors $\vec{m}_1$, $\vec{m}_2$ and amplitudes b_1, b_2. $\vec{X}$ is the horizontal position vector $\vec{i}\,x + \vec{j}\,y$. The corresponding wave numbers are $m_1 = |\vec{m}_1| = 2\pi/L_1$ and $m_2 = |\vec{m}_2| = 2\pi/L_2$, where L_1 and L_2 are the corresponding wavelengths. d is the mean depth of the sea bed and φ is the phase angle of the $\vec{m}_1$ component. To describe surface gravity water waves propagating over such a bottom topography, a Cartesian rectangular coordinate system is adopted with the $x-y$ plane coincident with the mean still water level and the z axis pointing vertically upwards. The origin is chosen so that the phase angle for the $\vec{m}_2$ component is zero. The fluid is assumed to be inviscid and incompressible, and the flow irrotational and represented by the velocity potential $\phi(x,y,z,t)$ that satisfies the Laplace equation over the entire flow field:

$$\nabla^2\phi = \phi_{xx} + \phi_{yy} + \phi_{zz} = 0 \quad \text{for } -d + b_1 \cos(\vec{m}_1 \cdot \vec{X} + \varphi) + b_2 \cos(\vec{m}_2 \cdot \vec{X}) \leqslant z \leqslant \eta, \tag{1}$$

where $\eta(x,y,t)$ is the elevation of the water surface. The fluid velocity can be derived from $\phi(x,y,z,t)$ by $\vec{V} = \nabla\phi = (\phi_x, \phi_y, \phi_z) = (u, v, w)$.

Let θ be the angle between the x-axis and the wavenumber vector of the incident wave $\vec{k}$. The incident wavenumber is $k = |\vec{k}| = 2\pi/L$, where L is its wavelength. θ_1 and θ_2 are the angles between the x-axis and the vectors $\vec{m}_1$ and $\vec{m}_2$, respectively, and the angle between these two vectors is defined as $\beta = \theta_2 - \theta_1$. Graphical descriptions of the progressive wave together with the coordinate system are depicted in Fig. 1.

It should be noted that the problem treated here can be extended to an arbitrary periodic bottom bathymetry because a sea bottom periodic in any two directions can be expressed as a superposition of two Fourier series.

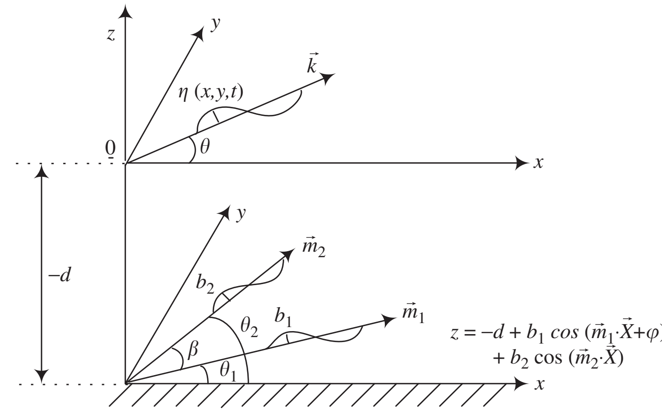

Fig. 1. Definition for a 3D wave motion system and a wavy bottom.

The boundary conditions on the free surface are:

(A) Free surface kinematic boundary condition (FSKBC)

$$\phi_z = \mathrm{d}\eta/\mathrm{d}t = \eta_t + \phi_x\eta_x + \phi_y\eta_y \text{ at } z = \eta(x, y, t), \text{ and} \tag{2}$$

(B) Free surface dynamic boundary condition (FSDBC)

$$\phi_t + g\eta + (\phi_x^2 + \phi_y^2 + \phi_z^2)/2 = 0 \text{ at } z = \eta(x, y, t), \tag{3}$$

where g is gravitational acceleration.

Besides, the bottom kinematic boundary condition that the fluid particles have zero velocity normal to the rigid bottom boundary has to be satisfied. That is, $\partial\phi/\partial n = \nabla\phi \cdot \vec{n} = \nabla\phi \cdot \nabla f/|\nabla f| = 0$, where $\vec{n}$ is the unit vector normal to the surface. After some manipulations, this bottom condition becomes

$$\phi_x\left[m_1 b_1 \cos\,\theta_1 \sin(\vec{m}_1 \cdot \vec{X} + \varphi) + m_2 b_2 \cos\,\theta_2 \sin(\vec{m}_2 \cdot \vec{X})\right] + \phi_y\left[m_1 b_1 \sin\,\theta_1 \sin(\vec{m}_1 \cdot \vec{X} + \varphi) + m_2 b_2 \sin\,\theta_2 \sin(\vec{m}_2 \cdot \vec{X})\right]$$
$$+ \phi_z = 0, z = -d + b_1 \cos(\vec{m}_1 \cdot \vec{X} + \varphi) + b_2 \cos(\vec{m}_2 \cdot \vec{X}). \tag{4}$$

An additional condition for the conservation of mass, combined with the periodicity of the bottom topography, is

$$\int_0^{2m\pi} \int_0^{2n\pi} \eta(x, y, t)\, \mathrm{d}(\vec{m}_1 \cdot \vec{X})\, \mathrm{d}(\vec{m}_2 \cdot \vec{X}) = 0. \tag{5}$$

Note that Eq. (5) is an integration with respect to non-dimensional quantities $\vec{m}_1 \cdot \vec{X}$ and $\vec{m}_2 \cdot \vec{X}$. The integer n is the ratio of the common multiple of L_1 and $L/\cos(\theta-\theta_1)$ to $L/\cos(\theta-\theta_1)$, and m is that of L_2 and $L/\cos(\theta-\theta_2)$ to $L/\cos(\theta-\theta_2)$. $L/\cos(\theta-\theta_1)$ and $L/\cos(\theta-\theta_2)$ represent the wavelength of the incident surface wave in the direction of $\vec{m}_1$ and $\vec{m}_2$, respectively. Graphical descriptions of this condition are shown in Fig. 2.

3. Theoretical Analysis

The FSKBC can be modified by combining with the FSDBC. First, multiply the FSKBC, (2), by g and then subtract it from the substantive (total) derivative of (3) with respect to t. The result, as presented in Longuet-Higgins (1962), is

$$\phi_{tt} + g\phi_z + 2\nabla\phi \cdot \nabla\phi_t + \nabla\phi \cdot \nabla(\nabla\phi)^2/2 = 0 \quad \text{at } z = \eta. \tag{6}$$

Note that both this condition and the FSDBC are established on the varying water level $z = \eta$ which is not known yet. Besides, the bottom boundary condition is set up on the undulating bottom $z = -d + b_1 \cos(\vec{m}_1 \cdot \vec{X} + \varphi) + b_2 \cos(\vec{m}_2 \cdot \vec{X})$. All these conditions should be expanded about $z = 0$ and $-$d, respectively, and Taylor series expansion should be utilized. These conditions, viz. Eqs. (3), (6) and (4) thus become

$$\phi_t + \eta\frac{\partial\phi_t}{\partial z} + \frac{1}{2}\eta^2\frac{\partial^2\phi_t}{\partial z^2} + g\eta + \frac{1}{2}(\nabla\phi)^2 + \eta\frac{\partial}{\partial z}\left[\frac{1}{2}(\nabla\phi)^2\right] + \text{HOT}\ldots = 0 \quad \text{at } z = 0, \tag{7}$$

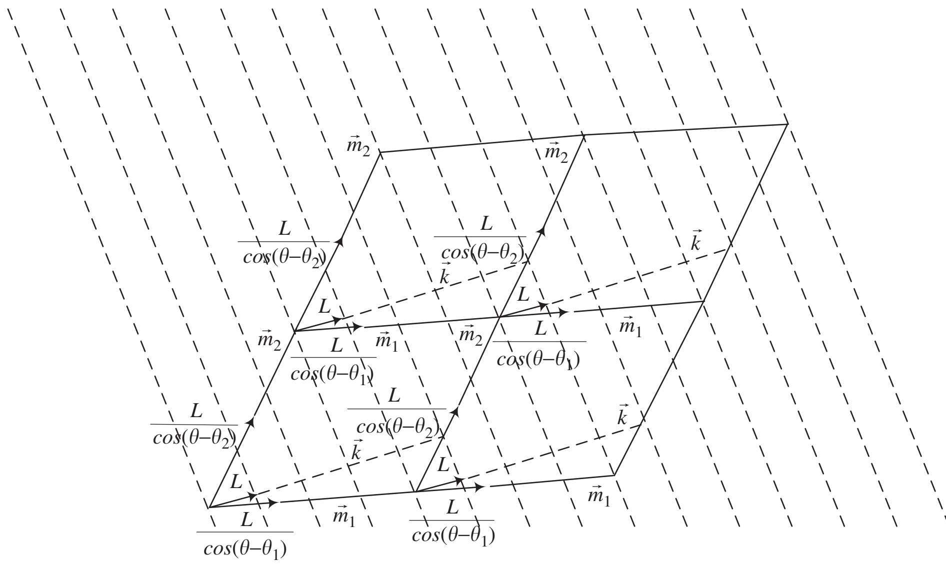

Fig. 2. Conservation of mass for the case of $n = 4$ and $m = 3$.

$$\phi_{tt} + \eta\frac{\partial\phi_{tt}}{\partial z} + \frac{1}{2}\eta^2\frac{\partial^2\phi_{tt}}{\partial z^2} + g\phi_z + \eta\frac{\partial(g\phi_z)}{\partial z} + \frac{1}{2}\eta^2\frac{\partial^2(g\phi_z)}{\partial z^2} + 2\nabla\phi\cdot\nabla\phi_t + \eta\frac{\partial(2\nabla\phi\cdot\nabla\phi_t)}{\partial z} + \frac{1}{2}\nabla\phi\cdot\nabla(\nabla\phi)^2$$
$$+\mathrm{HOT}\ldots = 0 \quad \text{at } z = 0. \tag{8}$$

$$\left[m_1 b_1 \cos\ \theta_1 \sin(\vec{m}_1\cdot\vec{X}+\varphi) + m_2 b_2 \cos\ \theta_2 \sin(\vec{m}_2\cdot\vec{X})\right] \times \left\{\phi_x + \left[b_1\cos(\vec{m}_1\cdot\vec{X}+\varphi) + b_2\cos(\vec{m}_2\cdot\vec{X})\right]\phi_{xz}\right.$$
$$\left. + \left[b_1\cos(\vec{m}_1\cdot\vec{X}+\varphi) + b_2\cos(\vec{m}_2\cdot\vec{X})\right]^2\phi_{xzz}/2\right\} + \left[m_1 b_1 \sin\ \theta_1 \sin(\vec{m}_1\cdot\vec{X}+\varphi) + m_2 b_2 \sin\ \theta_2 \sin(\vec{m}_2\cdot\vec{X})\right]$$
$$\times \left\{\phi_y + \left[b_1\cos(\vec{m}_1\cdot\vec{X}+\varphi) + b_2\cos(\vec{m}_2\cdot\vec{X})\right]\phi_{yz} + \left[b_1\cos(\vec{m}_1\cdot\vec{X}+\varphi) + b_2\cos(\vec{m}_2\cdot\vec{X})\right]^2\phi_{yzz}/2\right\}$$
$$+ \left\{\phi_z + [b_1\cos(\vec{m}_1\cdot\vec{X}+\varphi) + b_2\cos(\vec{m}_2\cdot\vec{X})]\phi_{zz} + \left[b_1\cos(\vec{m}_1\cdot\vec{X}+\varphi) + b_2\cos(\vec{m}_2\cdot\vec{X})\right]^2\phi_{zzz}/2\right\}$$
$$+\mathrm{HOT}\ldots = 0 \ \text{ at } \ z = -d. \tag{9}$$

From the boundary conditions, it is evident that the velocity potential ϕ, surface elevation η and angular frequency σ are all influenced by both the regular progressive gravity waves and the uneven bottom topography. Therefore the entire solutions can be written as the summation of these two contributions, viz. $\phi = \phi_w + \phi_b$, $\eta = \eta_w + \eta_b$, $\sigma = \sigma_w + \sigma_b$, where the subscript w denotes the contribution of the wave alone, and the subscript b denotes the bottom effect. In order to solve Eq. (1) together with boundary conditions (7)–(9), three small parameters are proposed: $\varepsilon_1 = a/L$ represents the steepness of the incident wave of amplitude a, while $\varepsilon_2 = b_1/L_1$ and $\varepsilon_3 = b_2/L_2$ represent the bottom slope. For convenience, the three different parameters are assumed to be of the same order $\varepsilon_1 \cong \varepsilon_2 \cong \varepsilon_3 \cong \varepsilon$. For example, a second order term may consist terms of components

$$O(a/L)^2 \cong \varepsilon_1^2 \cong \varepsilon^2,\ O(a/L)\times(b_1/L_1) \cong \varepsilon_1\varepsilon_2 \cong \varepsilon^2, O(a/L)\times(b_2/L_2) \cong \varepsilon_1\varepsilon_3 \cong \varepsilon^2,$$
$$O(b_1/L_1)^2 \cong \varepsilon_2^2 \cong \varepsilon^2 \text{ and } O(b_2/L_2)^2 \cong \varepsilon_3^2 \cong \varepsilon^2.$$

Note that this scale assumption is very general. When one parameter is significantly smaller than the other two, the solution so obtained is still correct to the same order. A simpler solution of the same accuracy can easily be obtained by dropping terms with this smaller parameter. The perturbative analysis is established by expanding the velocity potential ϕ, surface elevation η, and angular frequency σ as

$$\phi = \sum_{n=1}^{\infty}\phi_n = \phi_1 + \phi_2 + \phi_3 + \cdots$$
$$\eta = \sum_{n=1}^{\infty}\eta_n = \eta_1 + \eta_2 + \eta_3 + \cdots$$
$$\sigma = \sum_{n=0}^{\infty}\sigma_n = \sigma_0 + \sigma_1 + \sigma_2 + \cdots. \tag{10}$$

where the subscripts denote the order of magnitude associated with the perturbation analysis.

As the wave field fluctuates with σt, a specific quantity after differentiating with respect to t is magnified by σ. Following Chen (1989, 1990), a new variable $t_1 = \sigma t$ was proposed and the following chain rule was applied:

$$\frac{\partial\phi}{\partial t} = \frac{\partial\phi}{\partial t_1}\frac{\mathrm{d}t_1}{\mathrm{d}t} = \sigma\frac{\partial\phi}{\partial t_1}, \frac{\partial^2\phi}{\partial t^2} = \frac{\partial}{\partial t_1}\left(\frac{\partial\phi}{\partial t}\right)\frac{\mathrm{d}t_1}{\mathrm{d}t} = \sigma^2\frac{\partial^2\phi}{\partial t_1^2}$$

$$\text{viz.,}\quad \frac{\partial\phi}{\partial t} = \left(\sum_{n=0}^{\infty}\sigma_n\right)\frac{\partial\phi}{\partial t_1}, \frac{\partial^2\phi}{\partial t^2} = \left(\sum_{n=0}^{\infty}\sigma_n\right)^2\frac{\partial^2\phi}{\partial t_1^2}. \tag{11}$$

The governing equations, (1)–(5), can then be expanded and solved order by order, as will be shown in the following sections.

3.1. First-order approximation

The boundary-value problem correct to the first order is given by

$$\nabla^2\phi_1 = 0 \text{ for } -d \leqslant z \leqslant 0, \tag{12}$$

$$\sigma_0\phi_{1t_1} + g\eta_1 = 0 \text{ at } z = 0, \tag{13}$$

$$\sigma_0^2\phi_{1t_1t_1} + g\phi_{1z} = 0 \text{ at } z = 0, \tag{14}$$

$$\phi_{1z} = 0 \text{ at } z = -d, \tag{15}$$

$$\int_0^{2m\pi}\int_0^{2n\pi}\eta_1(x,y,t)\,\mathrm{d}(\vec{m}_1\cdot\vec{X})\,\mathrm{d}(\vec{m}_2\cdot\vec{X}) = 0, \tag{16}$$

and can be solved as

$$\phi_1 = \frac{ag}{\sigma_0}\frac{\cosh k(d+z)}{\cosh kd}\sin(\vec{k}\cdot\vec{X} - \sigma t + \delta), \tag{17}$$

$$\eta_1 = a\cos(\vec{k}\cdot\vec{X} - \sigma t + \delta), \tag{18}$$

$$\sigma_0^2 = gk\tanh kd, \tag{19}$$

where a is the amplitude of η_1 and δ is its phase angle at the origin $\vec{X} = 0$ and $t = 0$. The phase angle is chosen to be zero for convenience. The results are exactly a linear surface wave over constant water depth. Note that the bottom undulation has the same order as the velocity potential ϕ. Their interaction occurs in the second order and hence in the first order solution, the contribution of the parameters b_1/L_1 and b_2/L_2 are so small that the wavy bottom effect is not appreciable.

3.2. Second-order approximation

The governing equation and the boundary conditions of the problem, after substituting the first order solutions, are expressed as

$$\nabla^2\phi_2 = 0 \text{ for } -d \leqslant z \leqslant 0, \tag{20}$$

$$\sigma_0\phi_{2t_1} + g\eta_2 = \sigma_1\frac{ag}{\sigma_0}\cos(\vec{k}\cdot\vec{X} - \sigma t) - \frac{1}{4}\frac{a^2\sigma_0^2}{\sinh^2 kd} + \frac{k^2a^2g^2(2\sinh^2 - 1)}{4\sigma_0^2\cosh^2 kd}\cos 2(\vec{k}\cdot\vec{X} - \sigma t) \quad \text{at} \quad z = 0, \tag{21}$$

$$\sigma_0^2\phi_{2t_1t_1} + g\phi_{2z} = 2\sigma_1 ag\sin(\vec{k}\cdot\vec{X} - \sigma t) - \frac{3a^2g^2}{2\sigma_0\cosh^2 kd}\sin 2(\vec{k}\cdot\vec{X} - \sigma t)\text{at } z = 0, \tag{22}$$

$$\begin{aligned}\phi_{2z} = -\frac{ag}{2\sigma_0\cosh kd}\Big\{ & b_1\left[\vec{k}\cdot\vec{\lambda}_1^+\sin(\vec{\lambda}_1^+\cdot\vec{X} + \varphi - \sigma t) + \vec{k}\cdot\vec{\lambda}_1^-\sin(\vec{\lambda}_1^-\cdot\vec{X} + \varphi + t_1)\right] \\ & + b_2\left[\vec{k}\cdot\vec{\lambda}_2^+\sin(\vec{\lambda}_2^+\cdot\vec{X} - t_1) + \vec{k}\cdot\vec{\lambda}_2^-\sin(\vec{\lambda}_2^-\cdot\vec{X} + t_1)\right]\Big\}\text{at } z = -d,\end{aligned} \tag{23}$$

where $\vec{\lambda_i^{\pm}} = \vec{m}_i \pm \vec{k}$, $|\vec{\lambda_i^{\pm}}| = \lambda_i^{\pm}$, $i = 1\sim2$, and

$$\int_0^{2m\pi}\int_0^{2n\pi} \eta_2(x,y,t)\,\mathrm{d}(\vec{m}_1\cdot\vec{X})d(\vec{m}_2\cdot\vec{X}) = 0. \tag{24}$$

These equations can be solved for either non-resonant or resonant cases.

3.2.1. Non-resonant case

The second order solution of Eqs. (20)–(24) can be solved explicitly and the entire wave field, correct to the second order, can be written as

$$\sigma_1 = 0, \sigma = \sigma_w + \sigma_b = \sigma_0,\ \sigma_0^2 = gk\tanh kd, \tag{25}$$

$$\begin{aligned}\phi = \phi_1 + \phi_2 = {} & \frac{ag}{\sigma_0}\frac{\cosh\ k(d+z)}{\cosh\ kd}\sin(\vec{k}\cdot\vec{X} - \sigma t) + \frac{3}{8}\sigma_0 a^2\frac{\cosh\ 2k(d+z)}{\sinh^4 kd}\sin\ 2(\vec{k}\cdot\vec{X}-\sigma t)\\ & -\frac{1}{4}\left(\frac{\sigma_0^2 a^2 t}{\sinh^2 kd}\right) + \left(\frac{gab_1}{2\sigma_0\cosh\ kd}\right)\\ & \times\left\{\frac{\vec{k}\cdot\vec{\lambda_1^+}}{\lambda_1^+}\left[\frac{\lambda_1^+\cosh(\lambda_1^+ z) + k\tanh(kd)\sinh(\lambda_1^+ z)}{\cosh(\lambda_1^+ d)\left[\lambda_1^+\tanh(\lambda_1^+ d) - k\tanh(kd)\right]}\right]\sin(\vec{\lambda_1^+}\cdot\vec{X} - \sigma t + \varphi)\right.\\ & \left. + \frac{\vec{k}\cdot\vec{\lambda_1^-}}{\lambda_1^-}\left[\frac{\lambda_1^-\cosh(\lambda_1^- z) + k\tanh(kd)\sinh(\lambda_1^- z)}{\cosh(\lambda_1^- d)\left[\lambda_1^-\tanh(\lambda_1^- d) - k\tanh(kd)\right]}\right]\sin(\vec{\lambda_1^-}\cdot\vec{X} + \sigma t + \varphi)\right\}\\ & + \left(\frac{gab_2}{2\sigma_0\cosh\ kd}\right)\left\{\frac{\vec{k}\cdot\vec{\lambda_2^+}}{\lambda_2^+}\left[\frac{\lambda_2^+\cosh(\lambda_2^+ z) + k\tanh(kd)\sinh(\lambda_2^+ z)}{\cosh(\lambda_2^+ d)\left[\lambda_2^+\tanh(\lambda_2^+ d) - k\tanh(kd)\right]}\right]\sin(\vec{\lambda_2^+}\cdot\vec{X} - \sigma t)\right.\\ & \left. + \frac{\vec{k}\cdot\vec{\lambda_2^-}}{\lambda_2^-}\left[\frac{\lambda_2^-\cosh(\lambda_2^- z) + k\tanh(kd)\sinh(\lambda_2^- z)}{\cosh(\lambda_2^- d)\left[\lambda_2^-\tanh(\lambda_2^- d) - k\tanh(kd)\right]}\right]\sin(\vec{\lambda_2^-}\cdot\vec{X} + \sigma t)\right\} = \phi_w + \phi_b,\end{aligned} \tag{26}$$

$$\begin{aligned}\eta = \eta_1 + \eta_2 = {} & a\cos(\vec{k}\cdot\vec{X} - \sigma t)\\ & + ka^2\frac{(2\sinh^2 kd + 3)\cosh kd}{4\sinh^3 kd}\cos\ 2(\vec{k}\cdot\vec{X} - \sigma t)\\ & + \left(\frac{ab_1}{2\cosh\ kd}\right)\left\{\frac{(\vec{k}\cdot\vec{\lambda_1^+})\cos(\vec{\lambda_1^+}\cdot\vec{X} - \sigma t + \varphi)}{\cosh(\lambda_1^+ d)\left[\lambda_1^+\tanh(\lambda_1^+ d) - k\tanh(kd)\right]} - \frac{(\vec{k}\cdot\vec{\lambda_1^-})\cos(\vec{\lambda_1^-}\cdot\vec{X} + \sigma t + \varphi)}{\cosh(\lambda_1^- d)\left[\lambda_1^-\tanh(\lambda_1^- d) - k\tanh(kd)\right]}\right\}\\ & + \left(\frac{ab_2}{2\cosh\ kd}\right)\left\{\frac{(\vec{k}\cdot\vec{\lambda_2^+})\cos(\vec{\lambda_2^+}\cdot\vec{X} - \sigma t)}{\cosh(\lambda_2^+ d)\left[\lambda_2^+\tanh(\lambda_2^+ d) - k\tanh(kd)\right]} - \frac{(\vec{k}\cdot\vec{\lambda_2^-})\cos(\vec{\lambda_2^-}\cdot\vec{X} + \sigma t)}{\cosh(\lambda_2^- d)\left[\lambda_2^-\tanh(\lambda_2^- d) - k\tanh(kd)\right]}\right\} = \eta_w + \eta_b.\end{aligned} \tag{27}$$

Note that the first two terms of the velocity potential ϕ and the surface elevation η have nothing to do with the bottom topography. Hence, they represent the water wave effect and are respectively replaced by ϕ_w and η_w, where the subscript w denotes the contribution of the wave alone. The last two terms of ϕ and η are proportional to the bottom undulations b_1 and b_2, and are denoted by subscript b to represent the bottom effect. Thus, the complete ϕ and η can be expressed as the summation of two terms $\phi = \phi_w + \phi_b$ and $\eta = \eta_w + \eta_b$.

This solution is obtained by the regular perturbation method and the singularity, when the hyperbolic tangent terms in the denominator cancel each other, is not considered; thus, it is applicable only in the non-resonant case.

3.2.2. Resonant case

As is shown in Fig. 1, $0\leqslant\beta\leqslant\pi$ is the angle between $\vec{m}_1$ and $\vec{m}_2$. Let β_1 $(0\leqslant\beta_1\leqslant\pi)$ be the angle between $\vec{m}_1$ and $\vec{k}$, and β_2 $(0\leqslant\beta_2\leqslant\pi)$ be the angle between $\vec{m}_2$ and $\vec{k}$. Then, define $\lambda_i^{\pm} = |\vec{m}_i \pm \vec{k}|$, $m_i = |\vec{m}_i|$. It is easy to see that the denominators $\lambda_i^{\pm}\tanh(\lambda_i^{\pm}d) - k\tanh(kd)$, $i = 1, 2$, of both Eqs. (26) and (27) will equal to zero when $\lambda_i^{\pm} = k$. In this case, the second order terms tend to infinity and the solution becomes secular due to the resonance between the water wave and the sea bottom. This resonant condition can be stated as

$$\vec{\lambda}_i^{\pm} \cdot \vec{\lambda}_i^{\pm} = k^2 \quad \text{or} \quad \cos\ \beta_i = \mp\frac{m_i}{2k}\ ,\ \ i = 1\ ,2. \tag{28}$$

Under this resonant condition, the wavenumber vectors of the gravity wave and the wavy bottom can be sketched as shown in Fig. 3. Since $|\cos\ \beta_i|$ is less than or equal to unity, the resonance can occur only when $m_i \leqslant 2k$, as is predicted by Eq. (28). Fig. 3 also shows that $|\vec{m}_i - \vec{k}\,| = |\,\vec{k}\,|$ holds when $0 \leqslant \beta_i \leqslant \pi/2$, while $|\vec{m}_i + \vec{k}\,| = |\,\vec{k}\,|$ holds when $\pi/2 \leqslant 0 \leqslant \beta_I < \pi$. Of all four resonant cases that correspond to four variables $\lambda_i^{\pm} = |\vec{m}_i \pm \vec{k}\,|$, $i = 1{\sim}2$, in the resonant condition, only the solution for the case that involves $\lambda_1^- = |\vec{m}_1 - \vec{k}\,| = k$ and satisfies (28) is explicitly given in this section. All other cases can be solved in a similar way and the detail is not shown for brevity.

Hereafter, the symbols $\phi_r^{\pm(i)}$ for the velocity potential, $\eta_r^{\pm(i)}$ for the surface elevation, and $\sigma_r^{\pm(i)}$ for the angular frequency in which $i = 1, 2$ are used to denote the resonance with respect to the ith bottom ripple, respectively. The wave field that corresponds to the resonant condition $\lambda_1^- \tanh(\lambda_1^- d) - k \tanh(kd)$ is obtained following Chen (1992) as

$$\begin{aligned} &\sigma_{1r}^{-(1)} = 0, \\ &\sigma_r^{-(1)} = \sigma_w + \sigma_{br}^{-(1)} = \sigma_0, \sigma_0^2 = gk \tanh\ kd, \end{aligned} \tag{29}$$

$$\begin{aligned} \phi_r^{-(1)} = \phi_{1r}^{-(1)} + \phi_{2r}^{-(1)} = {} & \frac{ag}{\sigma_0}\frac{\cosh\ k(d+z)}{\cosh\ kd}\sin(\vec{k}\cdot\vec{X} - \sigma t) + \frac{3}{8}\sigma_0 a^2 \frac{\cosh\ 2k(d+z)}{\sinh^4 kd}\sin\ 2(\vec{k}\cdot\vec{X} - \sigma t) - \frac{1}{4}\left(\frac{\sigma_0^2 a^2 t}{\sinh^2 kd}\right) \\ & + \left(\frac{gab_1}{2\sigma_0 \cosh\ kd}\right)\left\{\frac{\vec{k}\cdot\vec{\lambda}_1^+}{\lambda_1^+}\left[\frac{\lambda_1^+ \cosh(\lambda_1^+ z) + k\tanh(kd)\sinh(\lambda_1^+ z)}{\cosh(\lambda_1^+ d)\left[\lambda_1^+ \tanh(\lambda_1^+ d) - k\tanh(kd)\right]}\right]\sin(\vec{\lambda}_1^+ \cdot \vec{X} - \sigma t + \varphi)\right. \\ & \left. + \frac{\vec{k}\cdot\vec{\lambda}_1^-}{\lambda_1^-}\left[e^{-\lambda_1^-(d+z)}\sin(\vec{\lambda}_1^- \cdot\vec{X} + \sigma t + \varphi)\frac{\vec{k}}{\lambda_1^+} - \frac{\cosh\ \lambda_1^-(d+z)}{\sinh\ 2kd}(\sigma t)\cos(\vec{\lambda}_1^-\cdot\vec{X} + \sigma t + \varphi)\right]\right\} + \left(\frac{gab_2}{2\sigma_0\cosh\ kd}\right) \\ & \times\left\{\frac{\vec{k}\cdot\vec{\lambda}_2^+}{\lambda_2^+}\left[\frac{\lambda_2^+\cosh(\lambda_2^+ z) + k\tanh(kd)\sinh(\lambda_2^+ z)}{\cosh(\lambda_2^+ d)\left[\lambda_2^+\tanh(\lambda_2^+ d) - k\tanh(kd)\right]}\right]\sin(\vec{\lambda}_2^+\cdot\vec{X} - \sigma t)\right. \\ & \left. + \frac{\vec{k}\cdot\vec{\lambda}_2^-}{\lambda_2^-}\left[\frac{\lambda_2^-\cosh(\lambda_2^- z) + k\tanh(kd)\sinh(\lambda_2^- z)}{\cosh(\lambda_2^- d)\left[\lambda_2^-\tanh(\lambda_2^- d) - k\tanh(kd)\right]}\right]\sin(\vec{\lambda}_2^-\cdot\vec{X} + \sigma t)\right]\right\} = \phi_w + \phi_{br}^{-(1)}\ ,\ \ \lambda_1^- = k, \end{aligned} \tag{30}$$

$$\begin{aligned} \eta_r^{-(1)} = \eta_{1r}^{-(1)} + \eta_{2r}^{-(1)} = {} & a\cos(\vec{k}\cdot\vec{X} - \sigma t) + ka^2\frac{(2\sinh^2 kd + 3)\cosh\ kd}{4\sinh^3 kd}\cos\ 2(\vec{k}\cdot\vec{X} - \sigma t) \\ & + \left(\frac{ab_1}{2\cosh\ kd}\right)\left\{\frac{(\vec{k}\cdot\vec{\lambda}_1^+)\cos(\vec{\lambda}_1^+\cdot\vec{X} - \sigma t + \varphi)}{\cosh(\lambda_1^+ d)\left[\lambda_1^+\tanh(\lambda_1^+ d) - k\tanh(kd)\right]} - \frac{\vec{k}\cdot\vec{\lambda}_1^-}{\lambda_1^-}\left[(e^{-\lambda_1^- d} - \frac{\operatorname{csch} kd}{2})\cos(\vec{\lambda}_1^-\cdot\vec{X} + \sigma t + \varphi)\right.\right. \end{aligned}$$

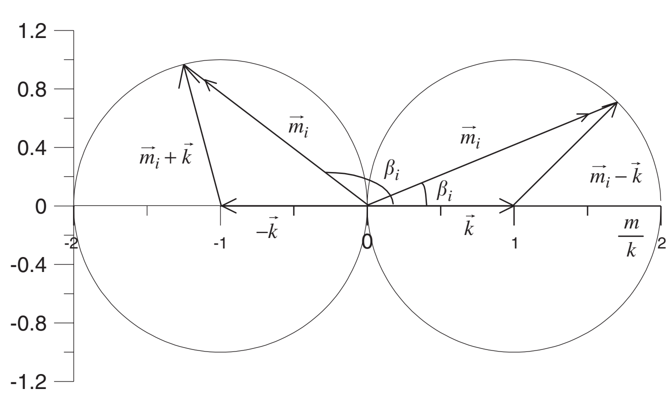

Fig. 3. Sketch of wave number vectors at resonance.

$$+\frac{\operatorname{csch} kd}{2}(\sigma t)\sin(\vec{\lambda}_1^- \cdot \vec{X} + \sigma t + \varphi)\Bigg]\Bigg\} + \left(\frac{ab_2}{2\cosh kd}\right)\Bigg\{\frac{(\vec{k}\cdot\vec{\lambda}_2^+)\cos(\vec{\lambda}_2^+\cdot\vec{X} - \sigma t)}{\cosh(\lambda_2^+ d)\left[\lambda_2^+ \tanh(\lambda_2^+ d) - k\tanh(kd)\right]}$$

$$-\frac{(\vec{k}\cdot\vec{\lambda}_2^-)\cos(\vec{\lambda}_2^-\cdot\vec{X} + \sigma t)}{\cosh(\lambda_2^- d)\left[\lambda_2^- \tanh(\lambda_2^- d) - k\tanh(kd)\right]}\Bigg\} = \eta_w + \eta_{br}^{-(1)}\ ,\ \ \lambda_1^- = k. \tag{31}$$

For other resonant cases, the mathematical expressions are similar to (30) and (31) and they can be easily obtained by changing the subscript and/or changing the minus sign to plus sign.

Note that in this paper, the perturbation theory is developed only to the second order. Thus, among the three perturbation parameters a/L, b_1/L_1 and b_2/L_2, only two of them couple together; that is, either a/L couples with b_1/L_1, or a/L couples with b_2/L_2. Consequently, the induced bottom effects can be obtained by directly superimposing terms of these two pairs of parameters.

3.2.3. Amplification with propagating distance

As was pointed out in Chen (1992), in resonance the water wave is amplified along with its traveling distance. This growth is related only to the resonant terms of the water wave solution (30) and (31)

$$\phi_{br'}^{-(1)} = -\frac{gab_1(\vec{k}\cdot\vec{\lambda}_1^-)}{4\sigma_0 k\sinh kd}\frac{\cosh k(d+z)}{\cosh^2 kd}(\sigma t)\cos(\vec{\lambda}_1^-\cdot\vec{X} + \sigma t + \varphi)\ ,\ \ \lambda_1^- = k,\ \text{and} \tag{32}$$

$$\eta_{br'}^{-(1)} = -\frac{ab_1(\vec{k}\cdot\vec{\lambda}_1^-)}{2k\sinh 2kd}(\sigma t)\sin(\vec{\lambda}_1^-\cdot\vec{X} + \sigma t + \varphi) \tag{33}$$

because all other terms do not grow.

The average energy flux of the resonant wave per unit wavelength, $\Delta F^{-(1)}$, can be obtained by employing the resonant velocity potential (32) as

$$\Delta F^{-(1)} = \frac{\rho}{2\pi}\int_0^{2\pi}\left\{\iint_{S_G}\left[\phi_{br'}^{-(1)}\right]_t\left[\nabla\phi_{br'}^{-(1)}\cdot\vec{n}^{-(1)}\right]ds\right\}d(\vec{\lambda}_1^-\cdot\vec{X}) = \frac{\rho}{2\pi}\int_0^{2\pi}\left\{\int_{z\approx -d}^{z\approx 0}\left[\phi_{br'}^{-(1)}\right]_t\left[\nabla\phi_{br'}^{-(1)}\cdot\frac{\vec{\lambda}_1^-}{\lambda_1^-}\right]dz\right\}d(\vec{\lambda}_1^-\cdot\vec{X})$$

$$= \frac{\rho g^2(\vec{k}\cdot\vec{\lambda}_1^-)^2 a^2 b_1^2(\sinh 2kd + 2kd)}{128\sigma_0^2 k^2\sinh^2 kd\cdot\cosh^4 kd}\sigma^3 t^2\ ,\ \ \lambda_1^- = k, \tag{34}$$

where ρ is the density of the fluid. S_G is an arbitrary vertical cross-section of unit width, extending from the sea bottom to the free surface. This means the integration is taken along the direction of resonant waves, in this case the direction of $\vec{m}_1 - \vec{k}$, from the bottom $z = -d + b_1\cos(\vec{m}_1\cdot\vec{X}) + b_2\cos(\vec{m}_2\cdot\vec{X})$ to the top $z = \eta$ in the vertical direction, and within a wavelength range that corresponds to phase $\vec{\lambda}_1^-\cdot\vec{X}$ ranging from 1 to 2π. The outward normal vector is defined as $\vec{n}^{-(1)} = (\vec{m}_1 - \vec{k})/|\vec{m}_1 - \vec{k}|$.

Based on the conservation of energy, $C_{gb}^{-(1)}$, which in resonance is the rate of energy transfer, should include both the incident group velocity C_g and a growth rate of energy flux due to resonance $\Delta C_g^{-(1)} = \Delta F^{-(1)}/E$. That is

$$\frac{C_{gb}^{-(1)}}{C_g} = 1 + \frac{\Delta C_g^{-(1)}}{C_g} = 1 + \frac{\Delta F^{-(1)}}{EC_g}, \tag{35}$$

where $E = \frac{1}{2}\rho g a^2$ is the averaged energy of the regular incident wave per unit width, and the group velocity C_g is given by linear wave theory as

$$C_g = \frac{d\sigma}{dk} = \frac{1}{2}\left(1 + \frac{2kd}{\sinh 2kd}\right)\frac{\sigma}{k}. \tag{36}$$

Substituting (34) and (36) into (35), the desired energy transfer velocity at resonance, $C_{gb}^{-(1)}$, can be obtained as

$$C_{gb}^{-(1)} = \left(1 + \frac{\Delta F^{-(1)}}{EC_g}\right)C_g = \left[1 + \frac{(\vec{k}\cdot\vec{\lambda}_1^-)^2 b_1^2\sigma^2 t^2}{4k^2\sinh^2 2kd}\right]C_g. \tag{37}$$

The growth of the resonant reflected wave with its traveling distance now is explicitly expressed by (37). The resonant wave has energy velocity $C_{gb}^{-(1)}$ and moves some distance $x_0^{-(1)}$ within the time t. The direction of $x_0^{-(1)}$ is the same as the direction of $C_{gb}^{-(1)}$, and both are identical to the resonant wave direction $\vec{m}_1 - \vec{k}$. The relationship between velocity, time, and distance gives

$$C_{gb}^{-(1)} = \frac{x_0^{-(1)}}{t} \text{ or } x_0^{-(1)} = C_{gb}^{-(1)} \cdot t. \tag{38}$$

Substituting the former equation into (37) and solving the resulting cubic equation for the unknown t, the relation between the displacement $x_0^{-(1)}$ and the corresponding time t is derived as

$$\begin{aligned} t = & \left\{ \frac{4k^3 x_0^{-(1)} \sinh^3 2kd}{(\vec{k}\cdot\vec{\lambda}_1^-)^2 b_1^2 \sigma^3 (\sinh\ 2kd + 2kd)} + \sqrt{\left[\frac{4k^3 x_0^{-(1)} \sinh^3 2kd}{(\vec{k}\cdot\vec{\lambda}_1^-)^2 b_1^2 \sigma^3 (\sinh\ 2kd + 2kd)}\right]^2 + \left[\frac{4k^2 \sinh^2 2kd}{3(\vec{k}\cdot\vec{\lambda}_1^-)^2 b_1^2 \sigma^2}\right]^3} \right\}^{1/3} \\ & + \left\{ \frac{4k^3 x_0^{-(1)} \sinh^3 2kd}{(\vec{k}\cdot\vec{\lambda}_1^-)^2 b_1^2 \sigma^3 (\sinh\ 2kd + 2kd)} - \sqrt{\left[\frac{4k^3 x_0^{-(1)} \sinh^3 2kd}{(\vec{k}\cdot\vec{\lambda}_1^-)^2 b_1^2 \sigma^3 (\sinh\ 2kd + 2kd)}\right]^2 + \left[\frac{4k^2 \sinh^2 2kd}{3(\vec{k}\cdot\vec{\lambda}_1^-)^2 b_1^2 \sigma^2}\right]^3} \right\}^{1/3}. \end{aligned} \tag{39}$$

After using (39), the growth of the resonant wave with time can then be represented as a form that grows with distance. The resonant terms of the velocity potential and the surface elevation become

$$\begin{aligned} \phi_{br'}^{-(1)} = & -\frac{g(\vec{k}\cdot\vec{\lambda}_1^-)ab_1}{2\sigma_0} \frac{\cosh\ k(d+z)}{\cosh\ kd} \cos(\vec{\lambda}_1^- \cdot \vec{X} + \sigma t + \varphi) \left\{ \left[\sqrt{\left(\frac{4x_0^{-(1)}}{(\vec{k}\cdot\vec{\lambda}_1^-)^2 b_1^2 (\sinh\ 2kd + 2kd)}\right)^2 + \left(\frac{4}{3(\vec{k}\cdot\vec{\lambda}_1^-)^2 b_1^2}\right)^3} \right. \right. \\ & \left. + \frac{4x_0^{-(1)}}{(\vec{k}\cdot\vec{\lambda}_1^-)^2 b_1^2 (\sinh\ 2kd + 2kd)} \right]^{1/3} + \left[\frac{4x_0^{-(1)}}{(\vec{k}\cdot\vec{\lambda}_1^-)^2 b_1^2 (\sinh\ 2kd + 2kd)} \right. \\ & \left. \left. - \sqrt{\left(\frac{4x_0^{-(1)}}{(\vec{k}\cdot\vec{\lambda}_1^-)^2 b_1^2 (\sinh\ 2kd + 2kd)}\right)^2 + \left(\frac{4}{3(\vec{k}\cdot\vec{\lambda}_1^-)^2 b_1^2}\right)^3} \right]^{1/3} \right\}, \end{aligned} \tag{40}$$

$$\begin{aligned} \eta_{br'}^{-(1)} = & -\frac{ab_1(\vec{k}\cdot\vec{\lambda}_1^-)}{2} \sin(\vec{\lambda}_1^- \cdot \vec{X} + \sigma t + \varphi) \times \left\{ \left[\sqrt{\left(\frac{4x_0^{-(1)}}{(\vec{k}\cdot\vec{\lambda}_1^-)^2 b_1^2 (\sinh\ 2kd + 2kd)}\right)^2 + \left(\frac{4}{3(\vec{k}\cdot\vec{\lambda}_1^-)^2 b_1^2}\right)^3} \right. \right. \\ & \left. + \frac{4x_0^{-(1)}}{(\vec{k}\cdot\vec{\lambda}_1^-)^2 b_1^2 (\sinh\ 2kd + 2kd)} \right]^{1/3} + \left[\frac{4x_0^{-(1)}}{(\vec{k}\cdot\vec{\lambda}_1^-)^2 b_1^2 (\sinh\ 2kd + 2kd)} \right. \\ & \left. \left. - \sqrt{\left(\frac{4x_0^{-(1)}}{(\vec{k}\cdot\vec{\lambda}_1^-)^2 b_1^2 (\sinh\ 2kd + 2kd)}\right)^2 + \left(\frac{4}{3(\vec{k}\cdot\vec{\lambda}_1^-)^2 b_1^2}\right)^3} \right]^{1/3} \right\}. \end{aligned} \tag{41}$$

In the resonant case, the complete wave field and surface elevation at a constant location x are

$$\phi_r^{-(1)}(x, y, t) = \phi_1 + \phi_{br'}^{-(1)}(x, y, t\,;\ x_0^{-(1)}) + \text{other non-resonant terms of (30)}, \tag{42}$$

$$\eta_r^{-(1)}(x, y, t) = \eta_1 + \eta_{br'}^{-(1)}(x, y, t\,;\ x_0^{-(1)}) + \text{other non-resonant terms of (31)} \tag{43}$$

4. Theory verification

In this study, a set of analytical solutions have been developed for waves propagating over a ripple bottom. To verify the mathematical results, the problem is reduced to simpler situations that can be compared with previous studies.

4.1. Extreme cases

The following two extreme cases can be easily shown to be satisfied:

(1) When the bottom becomes flat, $b_1 = b_2 = 0$, the solutions are successfully reduced to regular waves propagating over a uniform depth d.

(2) When the water is infinitely deep, $d \to \infty$, the bottom effect vanishes.

4.2. Bottom boundary condition

Up to the second-order solution derived in the previous section, it can be easily proven that the sea bottom is a streamline. This condition is always satisfied for arbitrary incident wave direction.

4.3. Reduced to unidirectional bottom topography

Comparing with field measurement or laboratorial tests is the most effective way to validate the accuracy of the present theory. However, there is no experiment that allows a wavy bottom to vary in two directions. Thus, the three-dimensional solution obtained in the previous sections should be reduced to a two-dimensional flow with just unidirectional bottom topography.

(1) *Singly sinusoidal topography*. The simplest unidirectional bottom topography has just one sinusoidal component and is a special case of the present study. Both the incident wave and the sand wave are of only one direction, the x-direction, and the following substitutions are used:

$$\begin{aligned}
&\vec{m}_1 = \vec{i}\, m_1 = \vec{i}\, m \ , \ b_2 = 0 \ , \ \vec{k} = \vec{i}\, k \ , \ \varphi = 0, \\
&\vec{X} = \vec{i}\, x \ , \ \theta = \theta_1 = 0, \\
&z = -d + b_1 \cos(\vec{m}_1 \cdot \vec{X} + \varphi) + b_2 \cos(\vec{m}_2 \cdot \vec{X}) = -d + b_1 \cos(mx), \\
&\vec{\lambda}_1^{\pm} = |\vec{m}_1 \pm \vec{k}\,| = |m \pm k| \ , \ \vec{k} \cdot \vec{\lambda}_1^{\pm} = k(m \pm k).
\end{aligned} \tag{44}$$

For the non-resonant case, the dispersion relation, velocity potential, and surface elevation are reduced to

$$\sigma_1 = 0, \quad \sigma = \sigma_w + \sigma_b = \sigma_0, \sigma_0^2 = gk \tanh\, kd, \tag{45}$$

$$\begin{aligned}
\phi = {} & \frac{ga}{\sigma_0} \frac{\cosh\, k(d+z)}{\cosh\, kd} \sin(kx - \sigma t) - \frac{1}{4}\left(\frac{a^2\sigma_0^2 t}{\sinh^2 kd}\right) + \frac{3}{8}\sigma_0 a^2 \frac{\cosh\, 2k(d+z)}{\sinh^4 kd} \sin\, 2(kx - \sigma t) + \frac{1}{2}\left(\frac{gkab_1}{\sigma_0 \cosh\, kd}\right) \\
& \times \left\{ \frac{(m+k)\cosh(m+k)z + k\tanh(kd)\sinh(m+k)z}{\cosh(m+k)d[(m+k)\tanh(m+k)d - k\tanh(kd)]} \sin[(m+k)x + \varphi - \sigma t] \right. \\
& \left. + \frac{(m-k)\cosh(m-k)z + k\tanh(kd)\sinh(m-k)z}{\cosh(m-k)d[(m-k)\tanh(m-k)d - k\tanh(kd)]} + \sin[(m-k)x + \varphi + \sigma t] \right\},
\end{aligned} \tag{46}$$

$$\begin{aligned}
\eta = {} & a\cos(kx - \sigma t) + \frac{ka^2}{4} \frac{(2\sinh^2 kd + 3)\cosh\, kd}{\sinh^3 kd} \cos\, 2(kx - \sigma t) \\
& + \frac{1}{2}\frac{ab_1 k}{\cosh\, kd} \left\{ \frac{(m+k)\cos[(m+k)x + \varphi - \sigma t]}{\cosh(m+k)d[(m+k)\tanh(m+k)d - k\tanh(kd)]} \right. \\
& \left. - \frac{(m-k)[\cos(m-k)x + \sigma t]}{\cosh(m-k)d[(m-k)\tanh(m-k)d - k\tanh(kd)]} \right\},
\end{aligned} \tag{47}$$

and the reflection coefficient is simply

$$R = \left| \frac{kb_1(1 - (2k/2m_1))\mathrm{sech}\,((2k/2m_1)m_1 b_1(d/b_1))\mathrm{sech}\,[(1 - (2k/2m_1))m_1 b_1(d/b_1)]}{2(1 - (2k/2m_1))\tanh[(1 - (2k/2m_1))m_1 b_1(d/b_1)] - (2k/2m_1)\tanh((2k/2m_1)m_1 b_1(d/b_1))} \right|. \tag{48}$$

If the Bragg resonance exists and the case $\lambda_1^- = |\vec{m}_1 - \vec{k}\,| = k$ is taken for example, the dispersion relation, velocity potential, and surface elevation are reduced to

$$\begin{aligned}
&\sigma_{1r}^{-(1)}\sigma_{1r} = 0, \\
&\sigma_r^{-(1)} = \sigma_r = \sigma_w + \sigma_{br} = \sigma_0, \sigma_0^2 = gk\tanh\, kd,
\end{aligned} \tag{49}$$

$$\begin{aligned}\phi_r^{-(1)} = \phi_r &= \frac{ag}{\sigma}\times\frac{\cosh\ k(d+z)}{\cosh\ kd}\sin(kx-\sigma t) - \frac{1}{4}\left(\frac{\sigma_0^2 a^2 t}{\sinh^2 kd}\right) + \frac{3}{8}\sigma_0 a^2 \frac{\cosh\ 2k(d+z)}{\sinh^4 kd}\sin\ 2(kx-\sigma t) + \frac{gab_1k}{2\sigma_0\cosh\ kd}\\ &\quad\times\left\{\frac{3k\cosh\ 3kz + k\tanh(kd)\sinh\ 3kz}{\cosh\ 3kd[3k\tanh\ 3kd - k\tanh(kd)]}\sin(3kx-\sigma t+\varphi) + \mathrm{e}^{-k(d+z)}\sin(kx+\sigma t+\varphi)\right.\\ &\quad\left. - \frac{\operatorname{csch} kd}{2\cosh\ kd}(\sigma t)\cosh\ k(d+z)\cos(kx+\sigma t+\varphi)\right\},\end{aligned} \tag{50}$$

$$\begin{aligned}\eta_r^{-(1)} = \eta_r &= a\cos(kx-\sigma t) + \frac{ka^2}{4}\frac{(2\sinh^2 kd+3)\cosh kd}{\sinh^3 kd}\cos\ 2(kx-\sigma t) + \frac{ab_1k}{2\cosh\ kd}\left\{\frac{3\cos(3kx-\sigma t+\varphi)}{\cosh\ 3kd[3\tanh(3kd) - k\tanh(kd)]}\right.\\ &\quad\left. - \left(\mathrm{e}^{-kd} - \frac{\operatorname{csch} kd}{2}\right)\cos(kx+\sigma t+\varphi) - \frac{\operatorname{csch} kd}{2}(\sigma t)\sin(kx+\sigma t+\varphi)\right\},\end{aligned} \tag{51}$$

and the reflection coefficient at resonance is reduced to

$$\begin{aligned}R_r(x_0^{-(1)}) &= \frac{1}{2}kb_1\left(\left\{\left[\frac{-4x_0^{-(1)}}{kb_1^2(\sinh\ 2kd+2kd)} + + \sqrt{\left(\frac{4x_0^{-(1)}}{kb_1^2(\sinh\ 2kd+2kd)}\right)^2 + \left(\frac{4}{3k^2b_1^2}\right)^3}\right]^{1/3}\right.\right.\\ &\quad\left.\left.\times\left[\frac{-4x_0^{-(1)}}{kb_1^2(\sinh\ 2kd+2kd)} - \sqrt{\left(\frac{4x_0^{-(1)}}{kb_1^2(\sinh\ 2kd+2kd)}\right)^2 + \left(\frac{4}{3k^2b_1^2}\right)^3}\right]^{1/3}\right\}^2 + \left[\frac{\mathrm{e}^{-2kd}}{\sinh\ 2kd}\right]^2\right).\end{aligned} \tag{52}$$

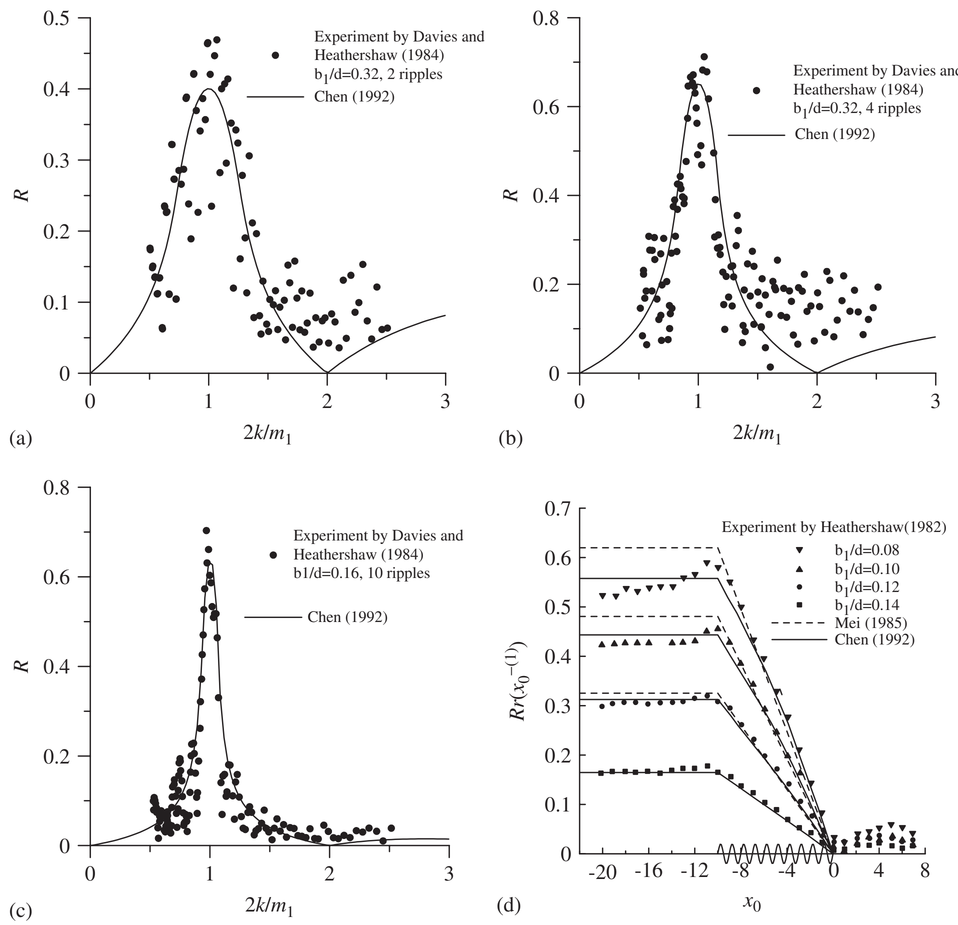

Fig. 4. Reflection coefficients over a singly sinusoidal topography: (a)–(c) are the comparison between the present theory, Eq. (48), and the experiments of Davies and Heathershaw (1984); (d) compares the present theory, Eq. (52), to the experiments of Heathershaw (1982) and the theory of Mei (1985).

The reduced results of Eqs. (45)–(52), are all coincident with Chen (1991,1992) which applied the same approach as the present study to waves propagating over a singly sinusoidal bottom. This 2-D flow field has been validated by comparing with the laboratorial experiments of Heathershaw (1982) and Davies and Heathershaw (1984) and the results are shown in Fig. 4, which are exactly the same as Figs. 2(a)–(c) and (d) of Chen (1992). In Figs. 4(a) and (b), where there are only two and four bottom ripples, the length of undulated bottom is so short that the bottom and the surface wave cannot fully interact, as is shown by the scattered experimental data. However, the average of the experimental reflection coefficient differs from the theoretical value for only 0.0039 in Fig. 4(a) and the averaged difference is 0.0553 in Fig. 4(b). There are 10 bottom ripples in Fig. 4(c) and the observed reflection coefficients are much more concentrated in the vicinity of the theoretical curve. In Fig. 4(d), the reflection coefficient is plotted during and after the ripple bottom zone for various ripple amplitude. The error between the experimental data and Chen's (1992) result is quite small: 3.87% for the case $b_1/d = 0.08$, 3.20% for $b_1/d = 0.10$, 2.13% for $b_1/d = 0.12$, and 2.55% for $b_1/d = 0.14$.

(2) *Doubly sinusoidal topography*. There are two ways to reduce the three-dimensional results to the doubly sinusoidal case where the wavy bottom has two sinusoidal components in the same direction. One way is by direct superposition of two singly sinusoidal solutions, and the other is by applying the following substitution:

$$
\begin{aligned}
&\vec{m}_1 = \vec{i}\, m \;,\; \vec{m}_2 = \vec{i}\, m \;,\; \vec{k} = \vec{i}\, k \;,\; \varphi = 0, \\
&\vec{X} = \vec{i}\, x \;,\; \theta = \theta_1 = 0, \\
&z = -d + b_1 \cos(\vec{m}_1 \cdot \vec{X} + \varphi) + b_2 \cos(\vec{m}_2 \cdot \vec{X}) = -d + b_1 \cos(mx) + b_2 \cos(mx), \\
&\vec{\lambda}_i^{\pm} = |\vec{m}_i \pm \vec{k}\,| = |m \pm k| \;,\; \vec{k} \cdot \vec{\lambda}_i^{\pm} = k(m \pm k) \;,\; i = 1{\sim}2.
\end{aligned}
\tag{53}
$$

The theoretical reflection coefficient then is plotted in Fig. 5 to compare with the experimental data of Guazzelli et al. (1992), and reasonable agreement is obtained. The dimensions of the bottom topography in each case are listed in Table 1, and the length of the ripple zone is 48 cm. The present theory predicts that the first order Bragg resonance will occur when either $2k = m_1$ or m_2 is satisfied, and this is consistent with the peak of the reflection coefficient in the experiment of Guazzelli et al. As demonstrated by Guazzelli et al. (1992), the second order superharmonic Bragg resonance occurs when $2k = 2m_1$, $2m_2$ or $m_1 + m_2$, while the subharmonic reflection occurs at $2k = m_1 - m_2$, $(m_1 > m_2)$. This higher order Bragg reflection cannot be predicted by the present theory and will be described in an extension of the present work to the third order (Cheng and Chen, 2005).

(3) *Obliquely incident waves*. The present theory describes the wave field propagating on a *bidirectionally periodic* bottom of arbitrary directions. To verify the theory, the present theory was simplified so that the bottom topography varies in the x-direction only. The resulting reflection coefficient is compared with Cho and Lee (2000) in Fig. 6. As incident angle θ

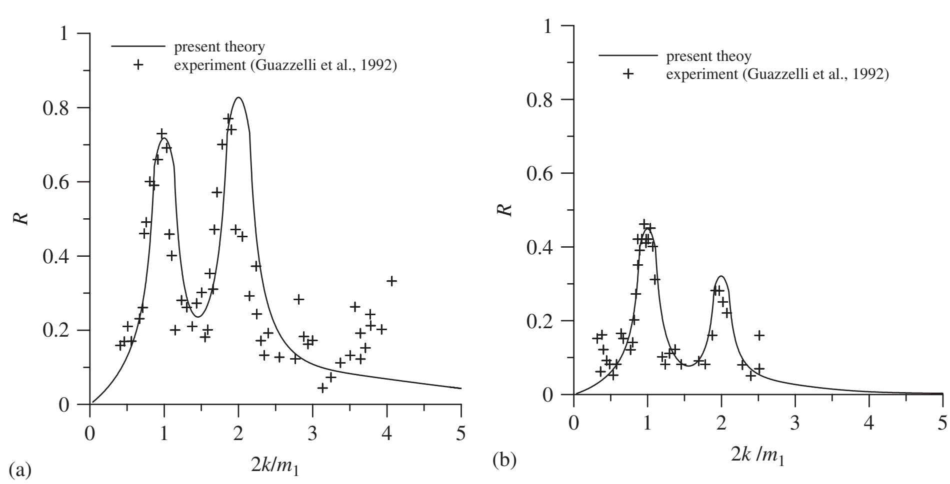

Fig. 5. Reflection coefficients over a doubly sinusoidal topography. The cross is the measurement of Guazzelli et al. (1992) and the solid line is the present theory.

Table 1
Dimensions of the doubly sinusoidal topographies of Fig. 5

	d(cm)	$b_1 = b_2$ (cm)	L_1 (cm)	L_2 (cm)
(a)	2.5	1.0	12.0	6.0
(b)	4.0	1.0	12.0	6.0

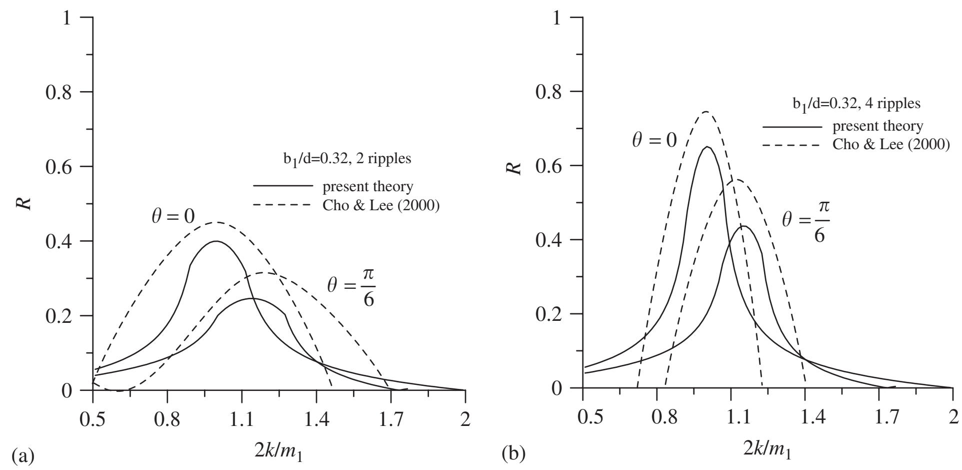

Fig. 6. Reflection coefficients for obliquely incident waves over singly sinusoidal topography.

increases, the reflection peak occurs for higher wave number k. The trend agrees with the numerical calculation of Cho and Lee (2000).

5. Discussion

5.1. The effect of the wavy bottom

In general non-resonant cases, the surface fluctuations deduced from undulated bottom topography decrease as the relative water depth d/L increases, and decrease as the ratio of b_1/d or b_2/d decreases. The bottom effects due to different incident angles θ and different ratios of L/L_1 or L/L_2 were controlled by the resonant conditions (28). For a specified ratio in which the bottom effects become more remarkable, the angle between the incident wave and any of the ripple wave vectors approaches the resonant angle calculated from the resonant condition (28) to a certain extent. The closer the incident angle is to the resonant angle, the more intensely the water surface rises and falls.

Fig. 7 exhibits the appearance of the resonant wave: (1) is the surface fluctuation due to the wavy bottom effect, (2) is the total surface elevation over wavy bottom, and (3) is the wavy bottom topography. In all three diagrams, the contours are shown on the left side, while the 3-D elevation is shown on the right.

The growth of the resonant wave can be seen from Fig. 8. As the relative water depth kd decreases, the resonant wave grows more significantly with both space and time.

6. Conclusions

This paper provides the mathematical derivations for three-dimensional progressive waves propagating over a bidirectionally sinusoidal bottom topography. By introducing three small perturbation parameters, the analytical solution correct to the second order is obtained. This result can be easily reduced to the two extreme cases of a flat bottom or infinitely deep water, and its agreement with the experimental data of Guazzelli et al. (1992) is reasonable. Thus, the accuracy and the generality of the explicit expressions are verified. Several concluding remarks and suggestions are

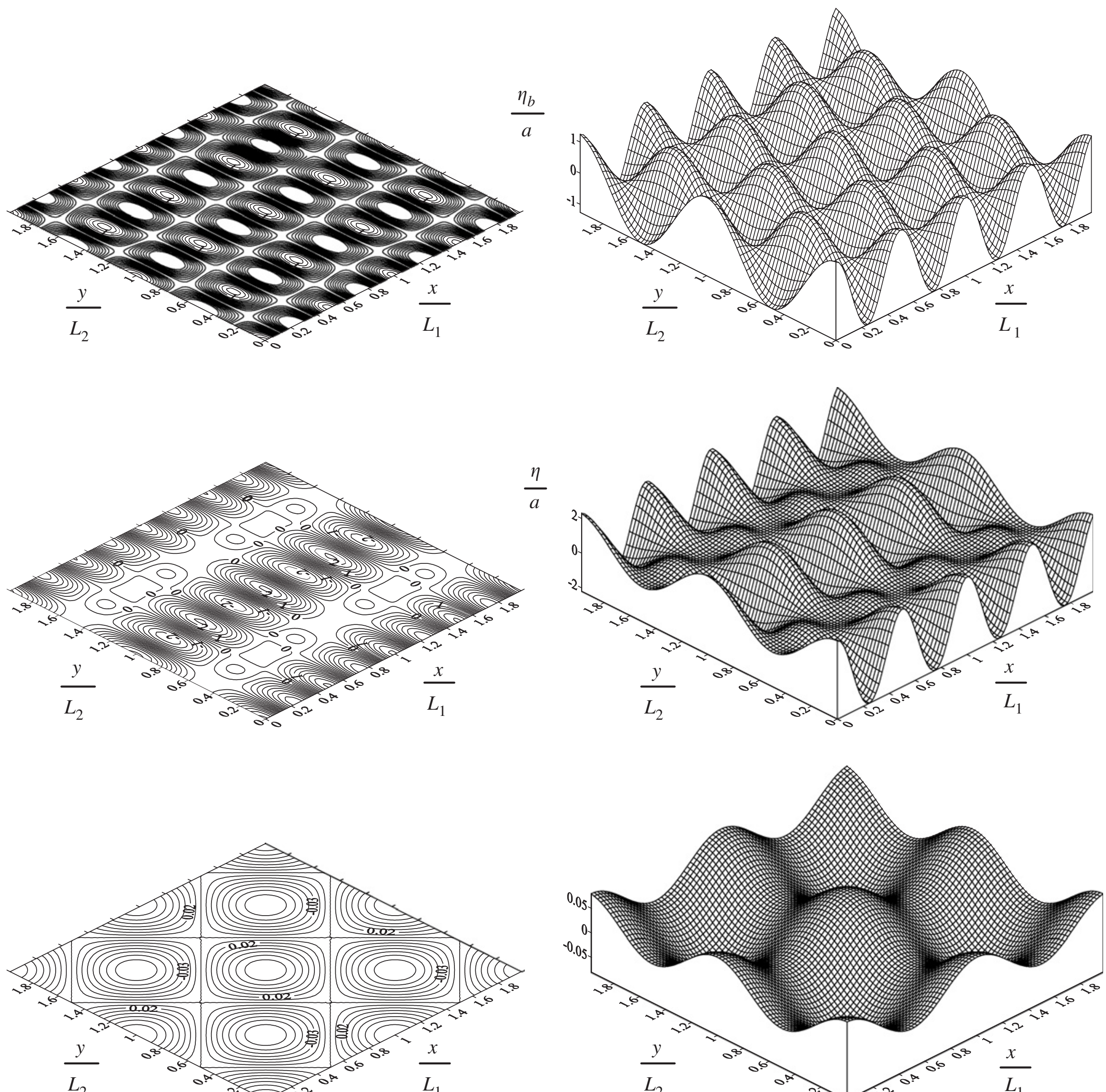

Fig. 7. The contour and the three-dimensional elevation of (1) the relative surface elevation due to the bottom effect η_b/a and (2) the relative total surface elevation η/a over a wavy bottom shown in (3). The wave and bottom conditions are $a/L = 0.01$, $d/L = 0.2$, $b_1/d = 0.2$, $b_2/d = 0.2$, $L/L_1 = 0.5$, $L/L_2 = 0.3$, $\theta = 0$.

given as follows:

1. The accuracy and the generality of the mathematical analysis can be firmly established. Although there are no suitable three-dimensional numerical solutions or laboratorial tests to compare with the results, it still can be successfully reduced to the two-dimensional situation and are consistent with previous research.
2. As can be easily understood, the effect of the bottom topography is more remarkable as the water depth becomes shallower, and the effect vanishes as the water depth becomes infinity.
3. Bragg resonance can occur when the incident wave travels over a bidirectionally periodic ripple bottom. The resonant condition can be explicitly derived from the secularity of the solution, and a separate resonant solution is found as well.
4. In the case of Bragg resonance, the growth rate of the energy flux and its relation to the traveling distance is explained. The resonant-motions also decay exponentially as the water depth increases and disappear in deep-water.
5. After reducing the three-dimensional results to two-dimensional, reasonable agreement with experiment is obtained.
6. The present study considers only a bottom of sinusoidal variation in two directions. However, when the real ripple bottom is idealized as being bidirectionally periodic, the bottom can always be treated as the superposition of sine and cosine functions and the bottom effect can be obtained by means of Fourier analysis. Therefore, this theory can be applied to a broad range of bottom bathymetries.

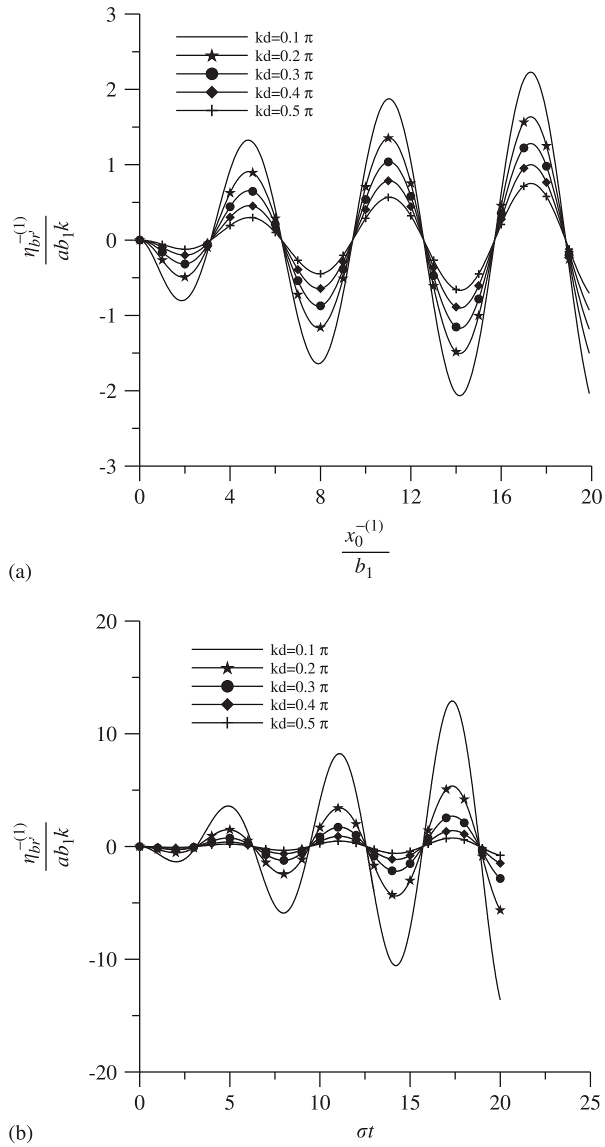

Fig. 8. Resonant wave grows with: (a) space; and (b) time with a zero incident angle θ.

Acknowledgments

This work was supported by research grants from Taiwan National Science Council under the project NSC93-2611-E-110-001.

APPENDIX A. NOTATION

The following symbols are used in this paper:

a	amplitude of incident waves
b_1	amplitude of bottom topography
b_2	amplitude of bottom topography
C_g	group velocity
$C_{gb}^{-(1)}$	energy transfer velocity at resonance
d	mean water depth
E	averaged energy of the regular incident wave per unit width
g	gravitational acceleration

k	wave number of incident waves
$\vec{k}$	wave number vector of incident waves
L	wavelength of incident waves
L_1	wavelength of bottom topography
L_2	wavelength of bottom topography
$\vec{m}_1$	wave number vector of bottom topography
$\vec{m}_2$	wave number vector of bottom topography
t	time
u	velocity component in x-direction
$\vec{V}$	velocity vector
v	velocity component in y-direction
w	velocity component in z-direction
$\vec{X}$	position vector
x,y,z	components of Cartesian rectangular coordinate
β	angle between $\vec{m}_1$ and $\vec{m}_2$
η	surface elevation
θ	angle between $\vec{k}$ and x-axis
θ_1	angle between $\vec{m}_1$ and x-axis
θ_2	angle between $\vec{m}_2$ and x-axis
ρ	density of fluid
σ	angular frequency
ϕ	velocity potential
φ	phase angle at origin

Subscripts:

x	partial derivative with respect to x
y	partial derivative with respect to y
z	partial derivative with respect to z
t	partial derivative with respect to t

References

Charberlain, P.G., Porter, D., 1995. Decomposition methods for wave scattering by topography with application to ripple beds. Wave Motion 22, 201–214.

Chen, Y.Y., 1989. Systematic approach to the interactions between two trains of gravity waves and its mechanism. Journal of Harbour Technology 4, 27–60 (in Chinese).

Chen, Y.Y., 1990. Nonlinear interaction between two gravity wave trains in water of uniform depth. Journal of Harbour Technology 5, 1–45 (in Chinese).

Chen, Y. Y., Tang, F. L. W., 1990. Analysis of regular progressive waves on ripple bottom. Proceedings of the 12th Ocean Engineering Conference, Taiwan, pp. 205–220 (in Chinese).

Chen, Y. Y., 1991. Bragg resonance for progressive gravity waves over a wavy bottom of finite length. Proceedings of the 15th National Conference on Theoretical and Applied Mechanics, Taiwan, pp. 289–296. (in Chinese).

Chen, Y.Y., 1992. Surface wave propagation over sinusoidally wavy bottom. Journal of Harbour Technology 7, 17–47 (in Chinese).

Cheng, C. Y., Chen, Y. Y., 2006. Analysis of regular progressive wave trains over ripple bottom, in preparation.

Cho, Y.S., Lee, C., 2000. Resonant reflection of waves over sinusoidally varying topographies. Journal of Coastal Research 16 (3), 870–876.

Davies, A.G., Heathershaw, A.D., 1984. Surface wave propagation over sinusoidally varying topography. Journal of Fluid Mechanics 144, 419–443.

Davies, A. G., 1980. Some interactions between surface water waves and ripples and dunes on the seabed. Inst. Oceanogr. Sci. Report 108.

Davies, A.G., 1982. On the interaction between surface waves and undulations on the seabed. Journal of Marine Research 40, 331–368.

Guazzelli, E., Rey, V., Belzons, M., 1992. Higher-order Bragg reflection of gravity surface waves by periodic beds. Journal of Fluid Mechanics 245, 301–317.

Hara, T., Mei, C.C., 1987. Bragg scattering of surface waves by periodic bars: theory and experiment. Journal of Fluid Mechanics 178, 221–241.

Heathershaw, A.D., 1982. Seabed-wave resonance and sand bar growth. Nature 296, 343–345.

Jeffreys, H., 1944. Motion of waves in shallow water, Note on the offshore bar problem and reflexion from a bar, Ministry of Supply Wave Report 3, London.

Kirby, J.T., 1986. A general wave equation for waves over rippled beds. Journal of Fluid Mechanics 162, 171–186.

Liu, Y., Yue, D.K.P., 1998. On generalized Bragg scattering of surface waves by bottom ripples. Journal of Fluid Mechanics 356, 297–326.

Longuet-Higgins, MS., 1962. Resonant interactions between two trains of gravity waves. Journal of Fluid Mechanics 12, 321–332.

Mei, C.C., 1985. Resonant reflection of surface water waves by periodic sand bars. Journal of Fluid Mechanics 152, 315–335.

Mei, C.C., Hara, T., Naciri, M., 1988. Note on Bragg scattering of water waves by parallel bars on the seabed. Journal of Fluid Mechanics 186, 147–162.

Mitra, A., Greenberg, M.D., 1984. Slow interactions of gravity waves and a corrugated sea bed. Transactions of the ASME E: J Appl Mech 51, 251–255.
Phillips, O.M., 1960. On the dynamics of unsteady gravity waves of finite amplitude. Part 1. Journal of Fluid Mechanics 9, 193–217.
Porter, R., Porter, D., 2001. Interaction of water waves with three-dimensional periodic topography. Journal of Fluid Mechanics 434, 301–335.
Rey, V., Guazzelli, E., Mei, C.C., 1996. Resonant reflection of surface gravity waves by one-dimensional doubly sinusoidal beds. Physics of Fluids 8 (6), 1525–1530.
Ursell, F., 1947. The reflection of waves from a submerged low reef. Admiralty Res. Lab., Teddington, Middx, Report ARL/R5/103.41/W.
Yu, J., Mei, C.C., 2003. Do Longshore Bars Shelter the Shore? Journal of Fluid Mechanics 404, 251–268.
Zhang, L., Kim, M.H., Edge, B.L., 1999. Hybrid model for Bragg scattering of water waves by steep multiply sinusoidal bars. Journal of Coastal Research 15 (2), 486–495.